ISSN 1330-3651 (Print), ISSN 1848-6339 (Online)
https://doi.org/10.17559/TV-20241212002191
Original scientific paper

A Novel Power Quality Improved Lead Acid Battery Charging System for the Electric Rickshaw

Sajitha BALARAMAN*, Vivekanandan CHENNIAPPAN

Abstract: Several thousands of electric rickshaws have been deployed in many of the Indian cities and the number of electric rickshaws deployed in various cities is growing day by day. The electric rickshaws invariably use 2 numbers of 12 V lead acid batteries. Most of the electric rickshaws commonly called E Rickshaws use domestic charging arrangements for charging the batteries and a variety of battery chargers is available in the market. This scenario has caused a great concern for the grid side power quality due to the nonlinear nature of the commercially available battery chargers which use rectifiers and filter capacitors. In this work a power factor corrected battery charging rectifier conforming to the charging pattern requirements of the lead acid batteries is presented. The control scheme ensures that the source current is of sinusoidal waveform. The proposed system uses a hysteresis controller and a sliding mode controller combination. The mathematical overheads and memory requirements in digital implementation of controller are minimal. The results of simulations carried out in the MATLAB SIMULINK environment and the results of the experimental prototype confirm and validate the efficacy of the proposed idea.

Keywords: cascaded buck boost converters; electric rickshaw battery chargers; hysteresis controller; lead acid battery chargers; power factor corrected rectifiers; sliding mode controllers; source current conditioning

1 INTRODUCTION

Battery charging is a traditional exercise and controlled or uncontrolled rectifiers have been widely used for this application. A step down transformer followed by a Diode Bridge Rectifier (DBR) followed by a filter capacitor is the basic form of a battery charger. But this arrangement offers no controllability and the harmonic pollution caused to the source in the form of harmonic currents is extremely high. The Silicon Controller Rectifier based battery charging units have also been popular. While this scheme offers a continuous controllability, it still pollutes the AC side of the system.

A good battery charger system particularly for applications such as the E Rickshaws which are used in a vastly distributed manner, individually used by the end user in an unpredictable schedule of charging hours is expected to draw sinusoidal source current at unity power factor and also it should follow the charging pattern for the specific battery as suggested by the battery manufacturer.

A number of battery charging topologies and control schemes have been presented by many researchers in the past and some of the milestone contributions have been outlined here so as to get an insight into the merits and demerits of the earlier systems.

The research article published in 1997 [1] discusses a method of pre estimating the total harmonics of the current drawn from the grid by the vast number of distributed battery chargers in a local area. The study gives an idea of estimation of the effects of harmonics and the actions to be taken about the mitigation of harmonics in grid. A similar study was carried out in the following year [2] with a particular focus on the harmonics based power quality pollution caused by EV battery charging systems. Such studies confirm the adverse effects of the everincreasing distributed battery charging systems on the quality of power in the grid caused by the variety of topologies and their respective control schemes [3].

In another development [4] a modular EV battery charging system that features a no dissipative current diverter has been presented. Yet another study on the impact of EV battery charging systems on the power quality of the grid has been carried out in [5]. A complete mathematical modelling of an E Vehicle battery charging system drawing power from the national power distribution system has been presented by the authors in [6]. The power quality related impact of the E vehicle chargers on the distribution system has been studied by the authors in [7]. A novel three phase powered E vehicle charging system that uses a boost rectifier topology has been proposed and validated by the authors in [8]. A comparison of the merits and demerits on the technical and economic considerations of distributed charging of E vehicle batteries as against using the battery swap centres has been done by the authors in [9]. A study of the battery driving behaviour with Electric vehicle and the charging behaviours has been systematically studied and recorded by the authors in [10]. This study helps the design and development of efficient and effective drives and chargers for the battery. A novel study of the demand profile of the battery of the E vehicle has been done under various charging options and has been presented in [11]. A comprehensive review of the RES based battery charging system has been done by the authors in [12]. In another development an intelligent EV charging system, considering the charging scheduling based on the charging characteristic of the battery has been developed in [13]. An optimal charging scheme suitable for the battery swapping center has been developed by the authors in [14]. The authors in [15] have developed the design and analysis of an optimal ZVS angle control for the charging of an EV battery using wireless power transfer principle. A power efficient energy management system that uses a solar PV source for charging a battery as well as exporting power to the distribution grid has been proposed and validated by the authors in [16]. In another development as reported in [17] an assessment of the performance has been carried out for a SEPIC converter based PFC rectifier for battery charging. A bridgeless Zeta converter based battery charging system has been presented in [18]. Considering all these developments and earlier contributions it has been observed that a power quality improved battery charger unit suitable for plug in type electrical vehicle charging is absolutely essential. The

charger must ensure that the source current is sinusoidal and the source side power actor is unity. Also the charging of the battery should follow the exact charging pattern as given by the manufacturer. Therefore, in this work, a power factor corrected battery charging system that charges the battery through the constant voltage and constant current phase automatically has been proposed. The proposed idea has been demonstrated using simulations in the MATLAB SIMULINK environment and an experimental setup. The article is arranged as different sections. Following this introduction as section 1 the second section gives an outline of the proposed system. The details of simulations in MATLAB SIMULINK are presented in section three. The Fourth section presents the details of the experimental prototype. The results obtained in the simulation and experimental prototype is discussed in section five. The conclusion and reference section are placed next.

2 OUTLINE OF THE PROPOSED SYSTEM

Fig. 1 shows the block schematic of the proposed system. Fig. 2 shows the topology of the proposed battery charger. Two series connected 12 V 35 AhLead Acid batteries are to be charged from the utility AC source. At the front end is a transformer rated 230/48 V, 50 Hz, 480 VA followed by a diode bridge rectifier (DBR). The usually used filtering capacitor is not used after the DBR. The output of the DBR is stepped up by a generic boost converter. The output port of the generic boost converter carries the filtering capacitor. The voltage across this capacitor is treated as the DC link voltage. A buck converter following the DC link charges the battery with the required voltage and current regulations as may be required. The manipulated parameters are the switching pulses applied to the boost converter and the buck converter. The boost converter control scheme ensures PFC operation with sinusoidal source current.

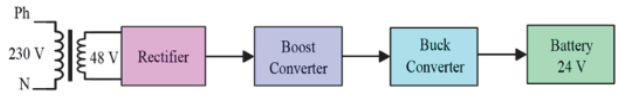

Figure 1 Block diagram of proposed system

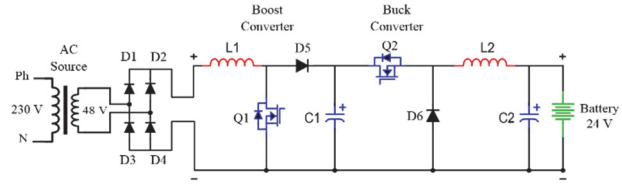

Figure 2 Topology of proposed system

Table 1 Specifications of the proposed system

System/Parameters	Specification
Main Source	1 Ph 50 Hz 48 V
Nominal Load	1000 W
Boost Converter Output	100 V
Nominal Battery Voltage	12V - 48 V
Inductor L_1	1 mH
Inductor L_2	1 mH
Capacitor	10000 µF

The buck converter control scheme takes care of the charging of the battery in the desired manner. The DC link voltage is more than 2 times the battery terminal voltage and the duty cycle of the buck converter can be adjusted flexibility to charge the battery with constant voltage or constant current modes. The special feature of the proposed system is that for the upkeep of the source side power factor, sinusoidal waveform of source current and for the regulation of the battery charging current in constant current mode or for the regulation of the battery terminal voltage during constant voltage mode, the sliding mode controller which is a variable structure controller and a hysteresis controller have been used. Some basic specifications of the system are given in Tab. 1. The proposed system has been developed in the MATLAB SIMULINK environment and the general system specifications are given in Tab. 1.

3 THE GENERIC BOOST CONVERTER

With a DC input voltage and given duty cycle the boost converter delivers a steady state DC output voltage. If the input voltage is time variant like a sinusoidal voltage wave and if a fixed duty cycle is used, then the output voltage should also be time varying. However, the filter capacitor on the output side may deliver a steady DC output voltage even if the input voltage is time varying like a sinusoidal source. The control system associated with the boost converter may be designed such that the AC source current becomes sinusoidal at unity power factor.

3.1 On the Front End Boost Converter

The front end converter of the proposed charger is the generic boost converter. The two storage elements of the generic boost converter are the boost inductor L_1 and the filter capacitor C_1. In this work the value of L_1 = 1 mH and C_1 = 10000 µF. The following buck converter and the battery can be considered as a continuously power drawing bulk resistor R with the output side capacitor C_2 and the buck section inductor L_2.

The input to the boost converter is the full wave rectified unfiltered DC derived from the front end DBR. The boost converter has one power control switch Q_1 and based on the On and Off states of this switch a set of voltage and current equations can be derived using Kirchhoff's voltage and current laws. These equations describe the state of the system in terms of the inductor current and the capacitor voltage when the switch is On and Off respectively.

In the case of the typical boost converter with the boost inductor L and the output capacitor C The scenario when the input voltage is Vs and the power electronic switch is in the On state can be described by Eq. (1) and Eq. (2).

$$V_s = L\frac{\mathrm{d}i_L}{\mathrm{d}t} \tag{1}$$

$$V_C = R \cdot C\frac{\mathrm{d}V_C}{\mathrm{d}t} \tag{2}$$

Similarly the scenario when the power electronic switch is turned Off can be described by Eq. (3) and Eq. (4).

$$V_C = V_S - L\frac{\mathrm{d}i_L}{\mathrm{d}t} \tag{3}$$

$$I_L = I_C + \frac{V_C}{R} \tag{4}$$

Based on Eq. (1) to Eq. (4) and the duty cycle D used for the On and Off state of the power control switch the average state space model can be derived. The average dstate space equation of the generic boost converter is shown Eq. (5).

There are two state variables namely the inductor current and the capacitor voltage. The state equation is given as Eq. (5) and the output is described by Eq. (6) where V_s is the source voltage, i_L is the inductor current, V_c is the capacitor voltage and D is the duty cycle.

$$\begin{bmatrix} \frac{\mathrm{d}i_L}{\mathrm{d}t} \\ \frac{\mathrm{d}V_C}{\mathrm{d}t} \end{bmatrix} = \begin{bmatrix} 0 & -\frac{1}{L} \\ \frac{1}{C} & \frac{-1}{RC} \end{bmatrix} \begin{bmatrix} i_L \\ V_c \end{bmatrix} + \begin{bmatrix} 0 & -\frac{1}{L} \\ \frac{1}{C} & -\frac{1}{RC} \end{bmatrix} \begin{bmatrix} D \\ V_s \end{bmatrix} \tag{5}$$

$$Y = CX \text{ and } Y = \begin{bmatrix} 0 & 1 \end{bmatrix} \begin{bmatrix} i_L \\ V_C \end{bmatrix} = V_C \tag{6}$$

The voltage gain of the generic boost DC to DC converter can be obtained by considering the state equation for the steady state when the rate of change of the state variables becomes zero and the voltage gain can be shown as Eq. (7).

$$\text{Voltage gain} = \frac{1}{(1-D)} \tag{7}$$

In Eq. (5) V_s is the input voltage and D is the duty cycle, i_L is the inductor current and V_c is the capacitor voltage. The state space equation shown byEq. (5) can be directly implemented in MATLAB SIMULINK as shown in Fig. 3.

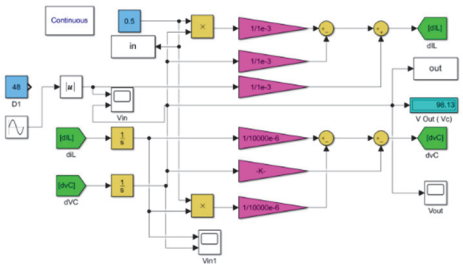

Figure 3 Average state space model of boost converter

The state space (SS) model as shown in Fig. 3 was tested with both AC and DC inputs separately and the dynamics of the state variables and the output were recorded and are shown in Fig. 4 to Fig. 7.The duty cycle was kept at 0,5 while the test was carried out. The capacitor voltage is the output voltage.

Fig. 5 to Fig. 7 show the waveforms corresponding to the case of DC voltage input of 48 V. After the transient state the state variables reach a steady state. It is observed that even if the source is time varying as derived from the DBR, with a fixed duty cycle the output voltage is a steady DC voltage as governed by the duty cycle. For an input of 48 V with a duty cycle of 0,5 the output voltage reaches the 96 V level. The voltage gain equation of the boost converter, as given in Eq. (7) reveals that the relation between the voltage gain and duty cycle is nonlinear. As for the buck converter, used in the battery side, and the converter this converter being a generic converter the voltage gain is given by the Eq. (8).

$$V_{\text{out}} = V_{\text{in}} D \tag{8}$$

As shown in Eq. (8) the voltage gain equation of the buck converter is linear and it passes through the origin. Since the source voltage of 48 V RMS is stepped up by the boost converter the DC link voltage is nearly 100 V and the nominal battery voltage is 24 V the buck converter can be used to charge the battery with either constant current mode or constant voltage mode. On the battery side the duty cycle of the buck converter is the manipulated variable. The control system does not use a conventional PWM generator with a fixed switching frequency but it uses a sliding mode controller that produces the switching pulses for the buck converter.

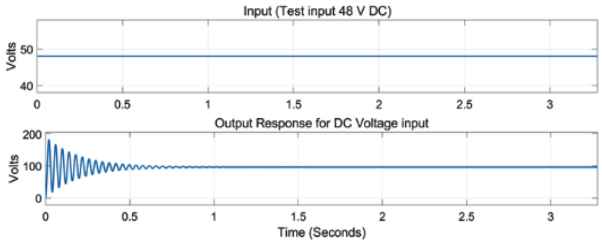

Figure 4 Input and output voltages of the SS model

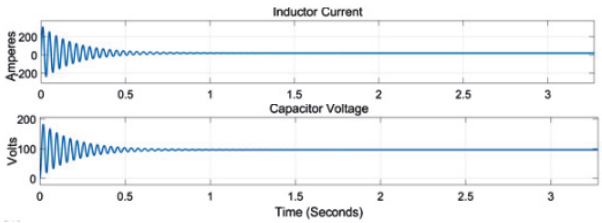

Figure 5 Trajectory of state variables

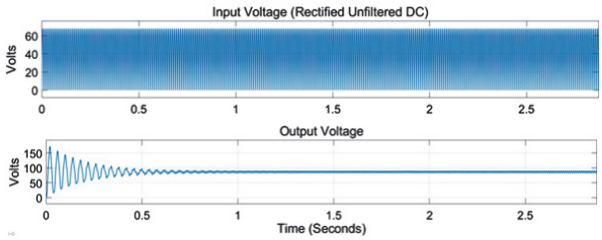

Figure 6 Input and its output response

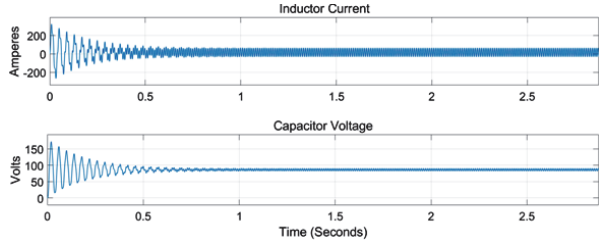

Figure 7 Trajectory of state variables

3.2 Charging Pattern of a Lead Acid Battery

The charging profile of a lead acid battery is shown in Fig. 8. Initially, the battery is charged in the constant current mode. During this period, the terminal voltage and the state of charge of the battery rise. As the terminal voltage of the battery reaches a specified value the mode of charging is changed from constant current mode to constant voltage mode. As the battery is charged in constant voltage mode the charging current reduces gradually.

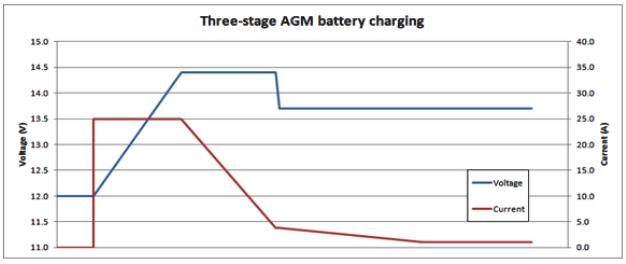

Figure 8 Charging profile

This is because of the gradual rise of the internal resistance of the battery. The internal resistance of the battery is in the order of 0,007 Ω for a typical 35 Ah 12 V battery. Therefore, the designed charger should be including control systems to charge the battery in the constant current mode with desired current and constant voltage mode with desired voltage. The control schemes for both constant current mode and constant voltage mode are discussed in this article.

4 REALIZATION IN MATLAB SIMULINK

The Proposed system was circuit modeled in the MATLAB SIMULINK environment and the sub systems realized in MATLAB are presented herein. Fig. 9 shows the overall block and Fig. 10 shows the boost converter sub system with the DBR at the front end. The output of the boost converter is terminated across the DC link capacitor. The DC link voltage is not regulated.

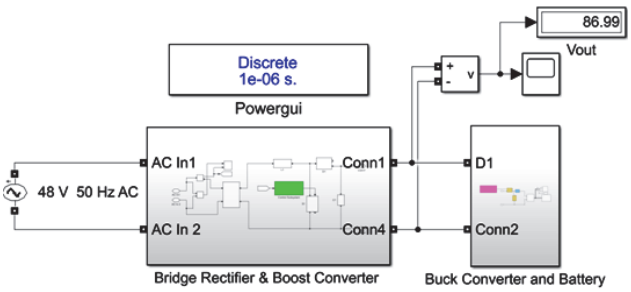

Figure 9 Complete block schematic of the proposed idea

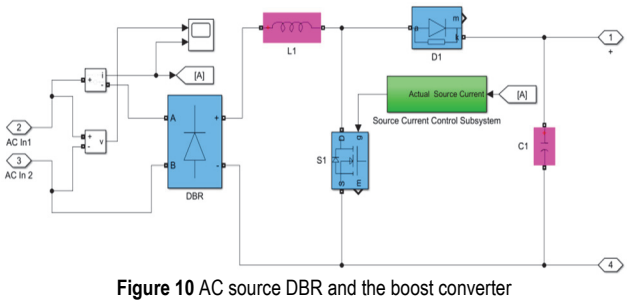

Figure 10 AC source DBR and the boost converter

The value of inductor is 1 mH and it ensures continuous conduction mode of operation. For a reduced ripple the DC link capacitor is 10000 μF and it ensures reduced ripple in the DC link voltage. The control section for the boost converter is shown in Fig. 11. With reference to Fig. 11, the control system estimates the required source current and compares it with the actual source current. Even though the source current is AC, the absolute value of the estimated source current and the absolute value of the actual source current are considered without considering their periodic polarity reversal. Since the source side power factor is to be kept at unity a sample of the source voltage is used as the unit template. The estimated source current waveform is obtained using the estimated RMS value of the source current and the unit template. The estimated reference current and the actual source current are used in a hysteresis comparator and the switching pulses are generated based on the instantaneous difference between the estimated source current and the actual source current. The error tolerance or bandwidth of ±0,1 is used in the hysteresis comparator. The RMS value of the source current required is estimated based on the desired battery charging current. Going by an example, if the desired battery charging current is 30 A then the power input to the battery for a nominal battery terminal voltage of 24 V is given by Eq. (9).

$$\text{Battery Power} = V_{\text{out}} \cdot I_{\text{bat}} \tag{9}$$

and it is 24 × 30 = 720 W. With the AC source voltage of 48 V 50 Hz RMS value the approximate value of source current can be found as follows. The single phase power is given in Eq. (10).

$$P_{AC} = VI\,Cos\,\varphi \tag{10}$$

Since expected power factor is unity Eq. (11) becomes (10).

$$P_{AC} = VI \tag{11}$$

and the RMS value of the source current can be calculated to be 15 A.

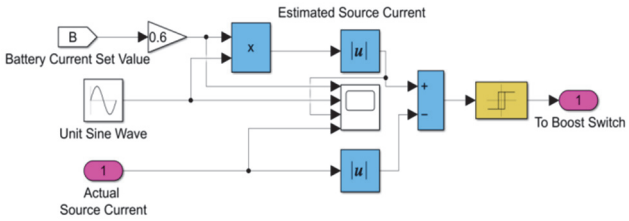

Figure 11 Control system used for the boost converter

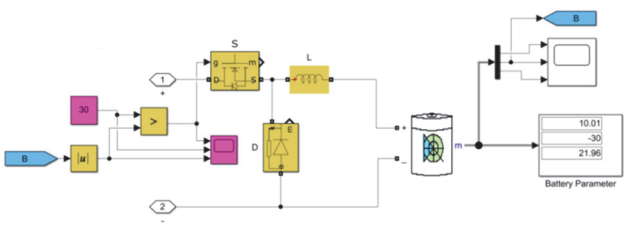

Figure 12 Battery side converter and control scheme

Thus the RMS value of the expected source current is obtained. Further, the battery side voltage is half the RMS value of the source side AC voltage. Therefore, under ideal lossless conditions the RMS value of the source current for any battery charging current is just half the battery charging current. In order to give allowance for losses and the possible variations on the source side voltage the RMS value of the source current is approximately 60% of the battery charging current. In this work this approximation has proved to be accurate for a wide range of battery charging currents. The results obtained for 10 A, 20 A and 30 A charging current as presented in the results section confirm the efficacy of this principle.

5 STABILITY OF THE PROPOSED SYSTEM

The proposed system constitutes a set of cascaded generic boost and buck converter units. The boost converter in the input side receives power from the unfiltered DBR. The output of the buck converter is connected to the battery for charging. When these two converters are set for operation simultaneously it is necessary to perform the stability analysis. Therefore, in this work, the stability of the proposed system has been studied in the open loop basis by using Bode plot, the root locus and the Nyquist plot. The transfer function between the output current I_{out} and the input voltage V_{in} has been estimated using MATLAB commands. With an input DC voltage of 24 V and the battery connected on the output of the buck converter with a duty cycle of 0,5 for the boost and the buck converters the transfer function has been estimated using the following commands in MATLAB command line.

>>mysys = iddata(I_{out}, V_{in}, 0,0001)
>>sys = tfest(mysys, 4)

These commands give the transfer function of the system as given in Eq. (12).

$$sys = \frac{364.9 \cdot S^3 - 3.107 \cdot 10^4 \cdot S^2 + 9.295 \cdot 10^6 \cdot s + 1.924 \cdot 10^7}{S^4 + 394 \cdot S^3 + 1.012 \cdot S^2 + 7.063 \cdot 10^6 \cdot S + 2.297 \cdot 10^8} \quad (12)$$

Based on this transfer function the root locus and the Nyquist plot were made as shown in Fig. 13 and Fig. 14.

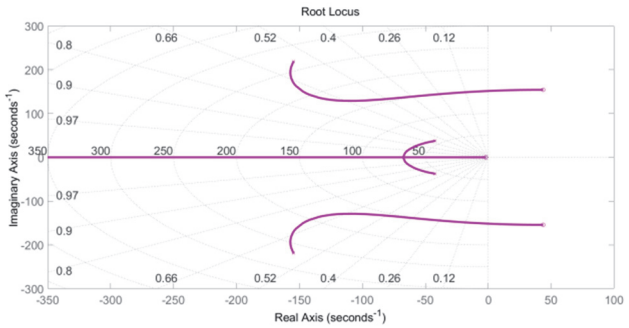

Figure 13 Root locus of the transfer function

The root locus reveals that all the poles are on the left hand half of the complex plane suggesting stability. In the Nyquist plot the −1 point along the *x* axis is not covered by the loops of the Nyquist plot and this feature confirms the stability of the system in the vicinity of the system with duty cycles of 0,5 applied to the boost and the buck converters.

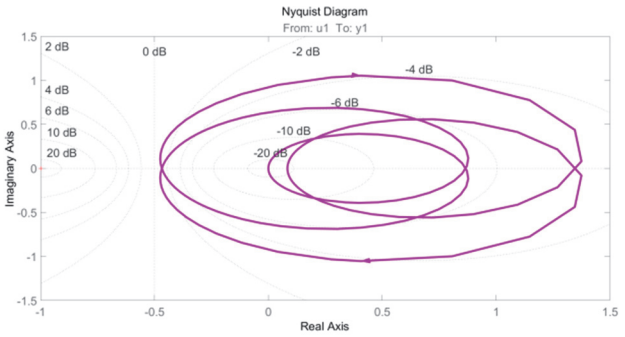

Figure 14 Nyquist plot of the transfer function

6 REALIZATION OF THE EXPERIMENTAL PROTOTYPE

An experimental setup was fabricated. The photograph of the experimental setup is shown in Fig. 15. There are two numbers of 12 V, 35 Ah lead acid batteries connected in series. For the boost converter MOSFET IRF840 has been used as the power control switch. For the buck converter MOSFET IRF540 has been used. The PIC micro controller 16F877A has been used as the digital controller. The incoming 230 V 50 Hz was stepped down to 48 V RMS using a 230/48 V 10 A transformer.

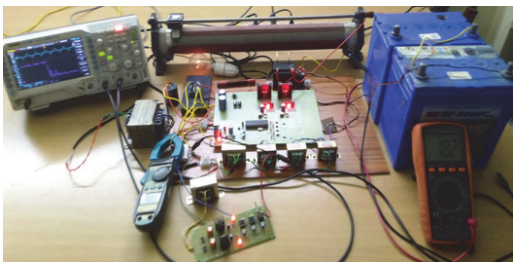

Figure 15 Photograph of the prototype

The capacity of the transformer is 480 VA. The batteries connected in series require a common nominal charging voltage just above 24 V and with a maximum charging current of 10 A the total real power required is 240 W. The front end rectifier is of the bridge type 25 A 500 V rectifier module. The isolation between the power electronic system and the control system is realized using optical isolation IC MCT 2E. The source current was monitored using a resistive current transducer and gives a signal corresponding to the source current. The sensor resistor was of value 0,047 Ω and with a current of 10 A flowing through this resistor the voltage drop would be 0,47 V. This low voltage signals corresponding to the source current is amplified to the 0 to 5 V level using the operation amplifier LM741. The circuit arrangement for providing bipolar power supply of +5V and −5 V to the LM 741 IC was also included. Some of the important waveforms are presented.

7 RESULTS AND DISCUSSIONS

Simulations as well as experimental verification are presented herein. To start with, the topology was tested

with a closed loop controller for the buck converter and the boost converter was removed as shown in Fig. 16.

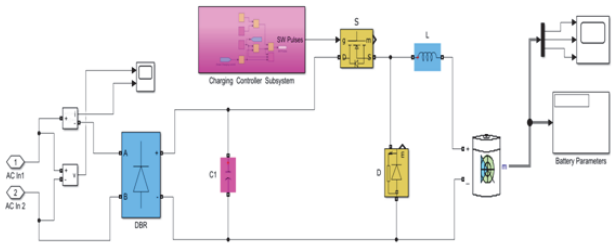

Figure 16 Battery charger with a DBR and a buck converter

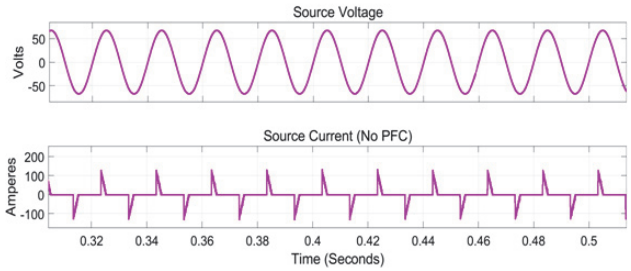

Figure 17 Source voltage and current without PFC

The filtered DC voltage output of the DBR is used by the buck converter. The PFC section is not in place. This causes the source side current to be highly nonlinear and the THD of the source current is also very high. The related waveforms are shown in Fig. 17 to Fig. 19. However, since the buck converter is in action on the battery side the charging current is regulated at 30 A with the constant current mode of charging as shown in Fig. 19.

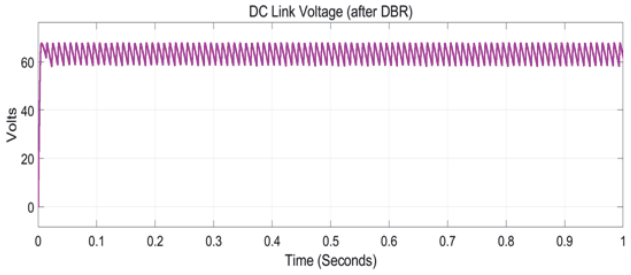

Figure 18 DC link voltage with DBR and filter

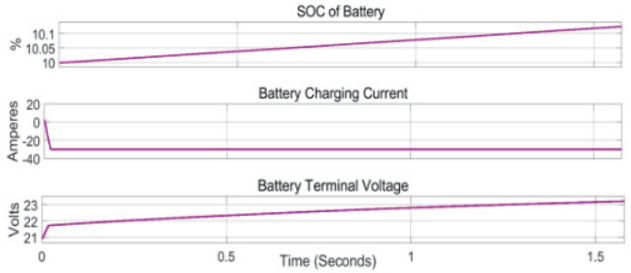

Figure 19 SOC, battery current and voltage

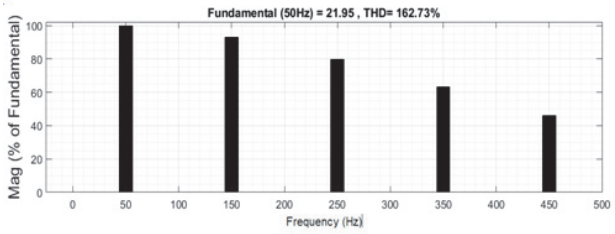

Figure 20 Harmonic spectrum of source current

This causes the SOC of the battery and the terminal voltage of the battery to rise as shown in Fig. 19. The only drawback with this method is the poor power quality on the source side with a high THD of 162,7% as shown in Fig. 20, The objective of this work is to develop a PFC rectifier at the front end that uses a generic boost converter in between the DBR and the final buck converter. Different charging currents like 10 A, 20 A and 30 A have been set and in all the cases the source side power factor stayed near unity and the source current THD was also less than the maximum allowable 5% limit as illustrated in the ongoing discussion.

8 CONSTANT CURRENT CHARGING

In simulations the battery was charged under constant current charging scheme with three different current settings viz. 10 A, 20 A and 30 A. In all these three cases the charging current was regulated at the desired values while the source current was maintained sinusoidal and the source side voltage and current were in phase leading to unity power factor. The DC link voltage, the switching pulses to the boost converter, the source voltage and current are shown in Fig. 21 to Fig. 23 respectively.

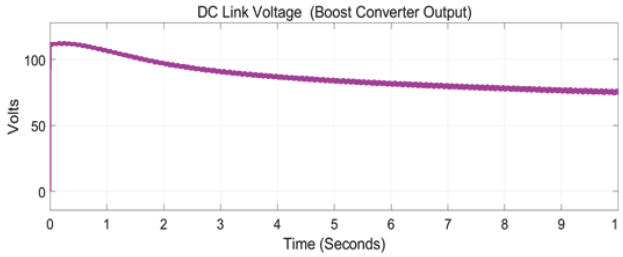

Figure 21 DC link voltage with PFC control

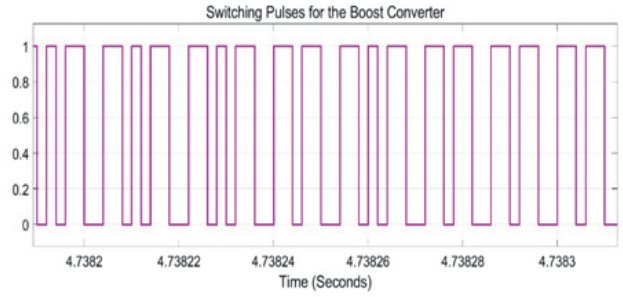

Figure 22 Switching pulses for the boost converter

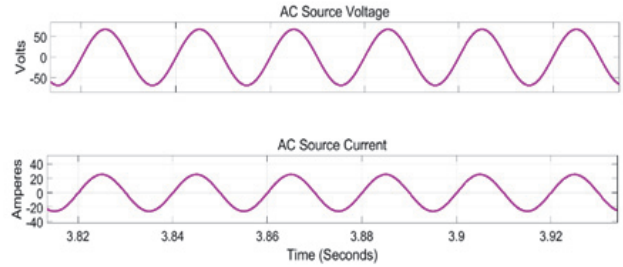

Figure 23 Source voltage and current

The waveforms related to the generation of the reference source current is shown in Fig. 24. Fig. 25 shows the rise of SOC of the battery, the battery current and the rising battery terminal voltage while charging. The reference source current is compared against the actual

source current and the switching pulses are generated by the hysteresis controller as shown in Fig. 26. On the battery side the buck converter regulates the charging current at the desired level as included in Fig. 26 wherein the set trajectory or desired waveforms of source current and the actual charging current are shown.

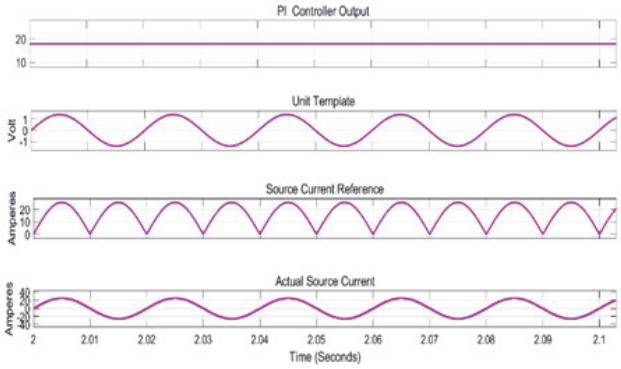

Figure 24 Generation of reference source current

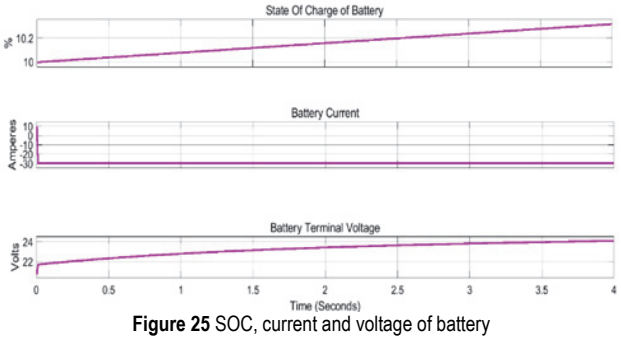

Figure 25 SOC, current and voltage of battery

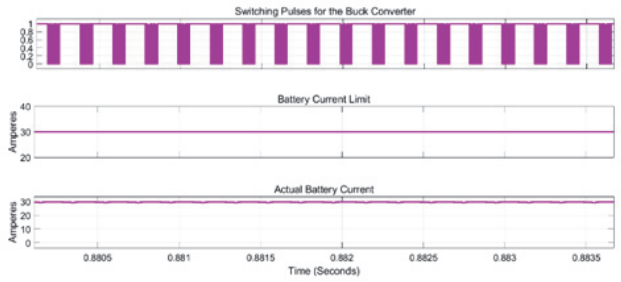

Figure 26 Switching pulses to the buck converter

The harmonic spectrum of the source current is shown in Fig. 27. For charging the battery with a charging current of 30 A the power is delivered to the battery while considering the nominal terminal voltage of the battery as 24 V is 24 × 30 = 720 W. On the input side the RMS value of the voltage is 48 V. The power factor is unity. The RMS value of the input current is therefore 720/48 = 15 A. This 15 A RMS source current is nearly sinusoidal with a THD as low as 1,63% as shown in Fig. 27.

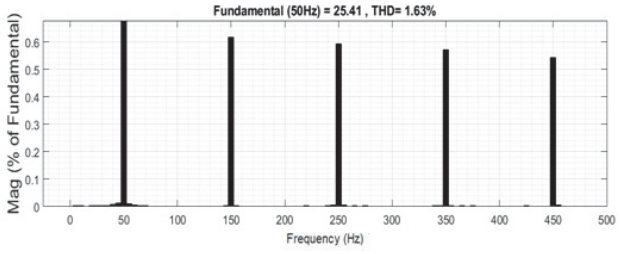

Figure 27 Harmonic spectrum of source current

In another experiment the battery charging current was set at 20 A. The nominal power input to the battery is therefore 480 W. The source current, for unity factor at 48 V RMS of the source side voltage, 10 A RMS with a peak value of 14,14 A as shown in Fig. 28. The switching pulses applied to the buck converter on the battery side, the set value of charging current and the actual charging current are shown in Fig. 29. The rise of the SOC of the battery and the terminal voltage of the battery are shown in Fig. 30. The THD of the source current is 1,18 and is shown in Fig. 31.

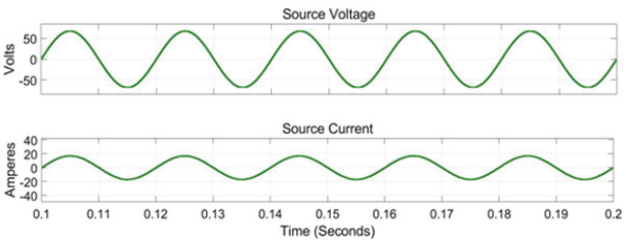

Figure 28 Source voltage and current

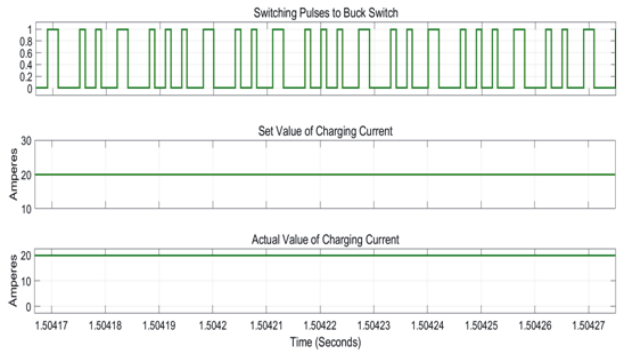

Figure 29 Switching pulses to buck converter

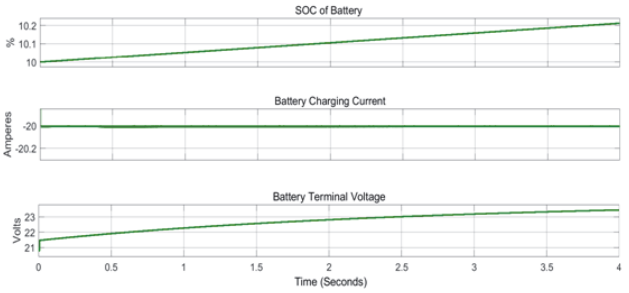

Figure 30 SOC, current and voltage of battery

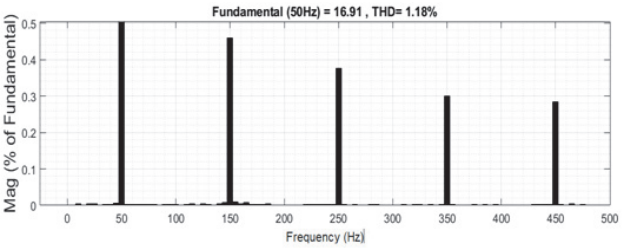

Figure 31 Harmonic spectrum of source current

The system was tested for a charging battery current of 10 A. At this condition the nominal input power to the battery was 240 W and this gives a source current of 5 A RMS at unity power factor and 48 V RMS on the AC side. The waveforms of the source voltage and current are shown in Fig. 32.

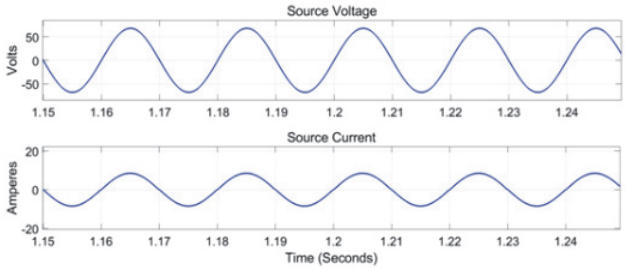

Figure 32 Source voltage and current

The switching pulses for the boost converter are generated by the hysteresis controller and the waveforms associated with this operation are shown in Fig. 33 and Fig. 34. The harmonic spectrum of the source current is shown in Fig. 35.

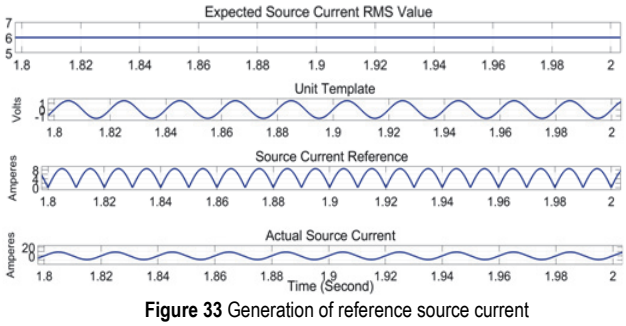

Figure 33 Generation of reference source current

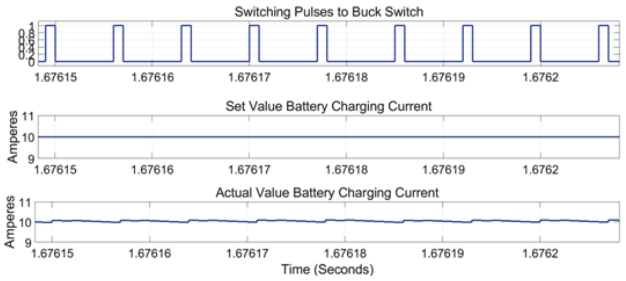

Figure 34 Switching pulses to buck converter

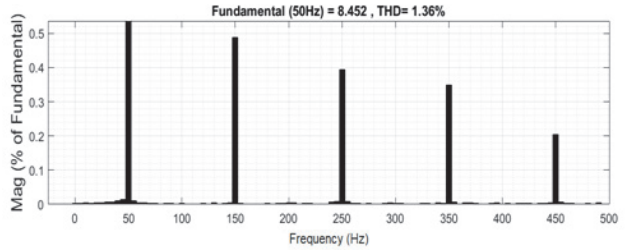

Figure 35 Harmonic spectrum of source current

9 CONSTANT VOLTAGE CHARGING

The system was tested with constant voltage charging also. During constant voltage charging the terminal voltage across the battery was held at the desired value and the charging current was not considered as a constraint. The constant voltage charging is done at a high SOC level of the battery and therefore the power delivered to the battery is low. The AC side source current is also reduced. The source current was however maintained sinusoidal with unity power factor. With constant voltage charging, since the battery internal resistance is very low the charging current may rise extremely high. In order to avoid this problem a charging current limiting is also included in the control scheme. The two cases of constant voltage charging with and without current limit were tested and the resulting waveforms are presented. With the constant voltage charging method, as the battery is getting charged, the internal resistance of the battery gets increased and this results in a gradual fall in the charging current. Even though the charging voltage remains fixed the fall in the charging current is caused by the rise of the internal resistance of the battery. The implementation of the control scheme for constant voltage charging MATLAB SIMULINK is shown in Fig. 36.

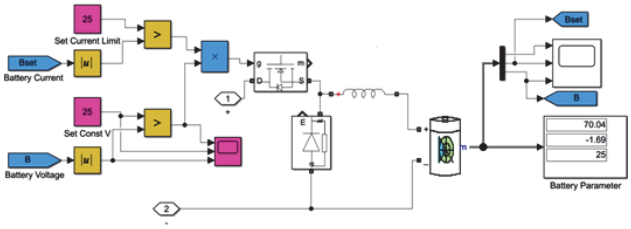

Figure 36 Control scheme for constant voltage charging with current limit

The various waveforms pertaining to constant voltage charging are given in Fig. 37 to Fig. 41. The terminal voltage across the battery, the charging current and the rise of the SOC and the source current waveforms are shown in Fig. 36 to Fig. 42. Fig. 36 shows the source voltage and current for constant voltage charging with the battery current that has limited the source AC current.

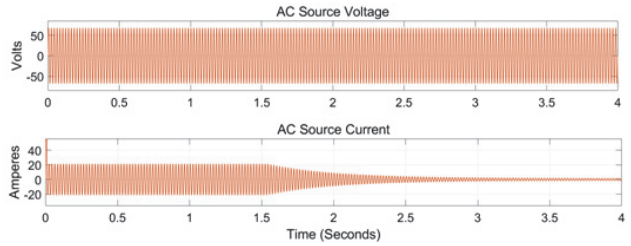

Figure 37 Source voltage and current

When power is turned on the energy storage devices, particularly the capacitors start charging initially drawing a large current and hence the source current is initially high. However, even the initial source current that is transiently large has also been maintained sinusoidal in waveform.

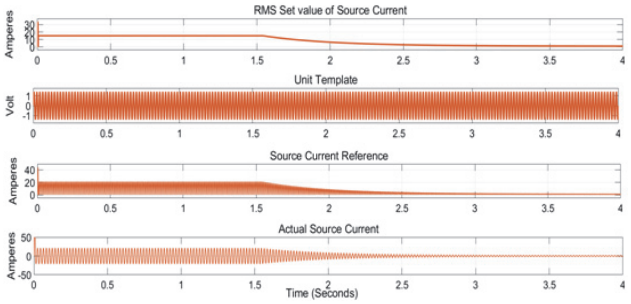

Figure 38 Reference current generation

With reference to Fig. 39, the battery being charged, the charging current is initially highly negative and as the battery terminal voltage rises and reaches the steady state of 25 V, from 1,5 seconds, the charging current is reduced. This reflects in the rate of rise of the SOC of the battery

which is initially high and then the rate of rise of SOC gets reduced.

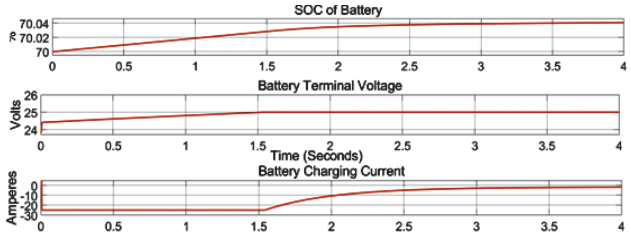

Figure 39 SOC battery voltage and current

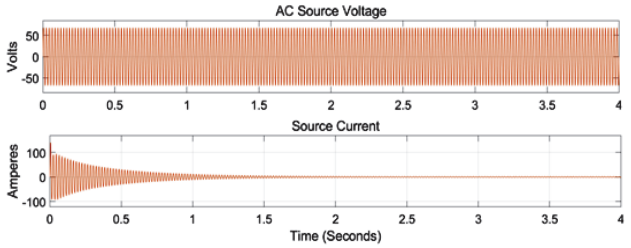

Figure 40 Source voltage and current (no current limit)

While charging the battery if there is no current limit is fixed, the source current is initially very high to the tune of 100 A and as the transients die out the source current gets reduced and reaches the steady state as shown in Fig. 40.The experimental setup was fabricated and tested for certain key operations. The experimental setup was first tested without the PFC control scheme and the resulting source current has been recorded and shown in Fig. 41. The harmonic spectrum shows the odd lower order harmonics and the THD is calculated to be 127%.

Figure 41 Source current without PFC

On the other hand, with PFC controller in place the source current was sinusoidal. The source current waveform and its harmonic spectrum are shown in Fig. 42. The THD was calculated to be 1,87%.

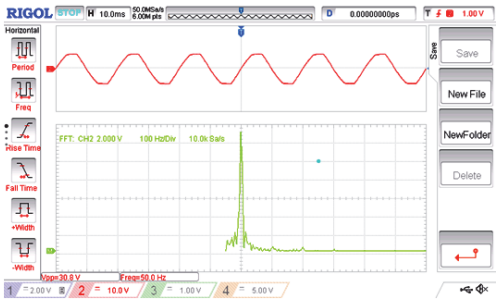

Figure 42 Source current with PFC

The ripple on the battery charging current was focused and the ripple in the charging current reflected the switching pulses applied to the buck converter. A ripple of 4,7 A peak to peak was observed for a charging current of 30 A as shown in Fig. 43. At this condition the terminal voltage of the battery was 22,8 V as shown in Fig. 44. A table of comparison of the power conversion efficiencies and power quality for different charging currents as observed from simulation and experimental prototype are presented in Tab. 2.

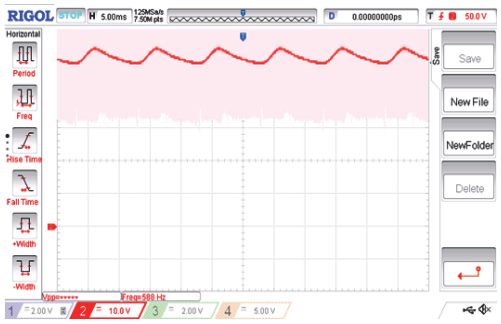

Figure 43 Battery charging current (zoomed)

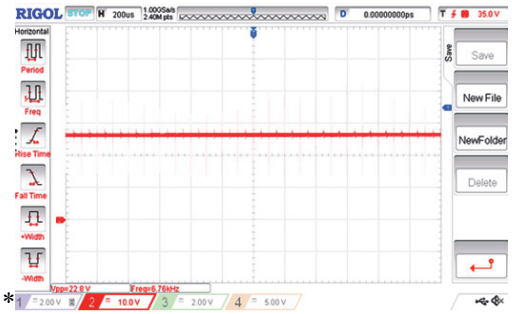

Figure 44 Battery terminal voltage

Table 2 Results

Simulation	Source PF	Source Current THD	Efficiency Boost	Efficiency Buck	B Current Ripple
Charging 10 A	0,91	1,36%	92%	91%	1,8 A PP
Charging 20 A	0,94	1,18%	93,5%	92%	2,6 A PP
Charging 30 A	0,97	1,63%	94%	94%	2,7 A PP
Prototype					
Charging 10 A	0,9	1,98%	86%	86%	3,6 A PP
Charging 20 A	0,91	2,3%	84%	85%	3,9 A PP
Charging 30 A	0,94	1,95%	82%	83%	4,7 A PP

10 CONCLUSION

A novel E Rickshaw battery charging system has been proposed and validated. Unlike the available chargers the charger has proved to offer two advantages. The first advantage is that it offers unity power factor on the source side AC current with near sinusoidal source current with THD in the range of 0,75% to 1,5% for different charging

currents and the observed THD is much less from the allowable 5% limit. The performance has been tested with a charging battery current of 10 A, 20 A and 30 A in simulations and the source current power quality has been observed to be satisfactory for all ranges of charging current. In addition, the system does not require tedious mathematical modeling and it has not used classical controllers like the PI controller, the fuzzy logic controller nor any advanced controllers like the ANFIS or the ANN based controllers. This work has focused on developing a practical charging system for high potential markets, eliminating mathematical overheads and using classical theories. The developed simulations and the results of the prototype prove the efficacy of the proposed idea.

11 REFERENCES

[1] Staats, B., Grady, P. T., Arapostathis, A., & Thallam, R. S. (1997). A statistical method for predicting the net harmonic currents generated by a concentration of electric vehicle battery chargers. *IEEE Transactions on power Delivery*, *12*(3), 1258-1266. https://doi.org/10.1109/61.637002

[2] Staats, B., Grady, P. T., Arapostathis, A., & Thallam, R. S. (1998). A statistical analysis of the effect of electric vehicle battery charging on distribution system harmonic voltages. *IEEE Transactions on Power Delivery*, *13*(2), 640-646. https://doi.org/10.1109/61.660951

[3] Kutkut, N. H. (1998). A modular no dissipative current diverter for EV battery charge equalization. *APEC'98 Thirteenth Annual Applied Power Electronics Conference and Exposition*, *2*, 686-690). https://doi.org/10.1109/APEC.1998.653973

[4] Gómez, J. C. & Morcos, M. M. (2003). Impact of EV battery chargers on the power quality of distribution systems. *IEEE transactions on power delivery*, *18*(3), 975-981. https://doi.org/10.1109/TPWRD.2003.813873

[5] Qian, K., Zhou, C., Allan, M., & Yuan, Y. (2010). Modeling of load demand due to EV battery charging in distribution systems. *IEEE transactions on power systems*, *26*(2), 802-810. https://doi.org/10.1109/TPWRS.2010.2057456

[6] Rutherford, M. J. & Yousefzadeh, V. (2011). The impact of electric vehicle battery charging on distribution transformers. *2011 Twenty-Sixth Annual IEEE Applied Power Electronics Conference and Exposition (APEC)*, 396-400). https://doi.org/10.1109/APEC.2011.5744627

[7] Lee, J. H., Moon, J. S., Lee, Y. S., Kim, Y. R., & Won, C. Y. (2011). Fast charging technique for EV battery charger using three-phase AC-DC boost converter. *IECON 2011 - 37th Annual Conference of the IEEE Industrial Electronics Society*, 4577-4582. https://doi.org/10.1109/IECON.2011.6120064

[8] Worley, O. & Klabjan, D. (2011). Optimization of battery charging and purchasing at electric vehicle battery swap stations. *2011 IEEE vehicle power and propulsion conference*, 1-4. https://doi.org/10.1109/VPPC.2011.6043182

[9] Smart, J. & Schey, S. (2012). Battery Electric Vehicle Driving and Charging Behavior Observed Early in the EV project. *SAE International Journal of Alternative Powertrains*, *1*(1), 27-33. https://doi.org/10.4271/2012-01-0199

[10] Marra, F., Yang, G. Y., Traeholt, C., Larsen, E., Rasmussen, C. N., & You, S. (2012). Demand profile study of battery electric vehicle under different charging options. *2012 IEEE power and energy society general meeting*, 1-7. https://doi.org/10.1109/PESGM.2012.6345063

[11] Huang, Z., Wong, S. C., & Chi, K. T. (2016). Design of a single-stage inductive-power-transfer converter for efficient EV battery charging. *IEEE Transactions on Vehicular Technology*, *66*(7), 5808-5821. https://doi.org/10.1109/TVT.2016.2631596

[12] Sujitha, N. & Krithiga, S. (2017). RES based EV battery charging system: A review. *Renewable and Sustainable Energy Reviews*, *75*, 978-988. https://doi.org/10.1016/j.rser.2016.11.078

[13] Wei, Z., Li, Y., Zhang, Y., & Cai, L. (2017). Intelligent parking garage EV charging scheduling considering battery charging characteristic. *IEEE transactions on industrial electronics*, *65*(3), 2806-2816. https://doi.org/10.1109/TIE.2017.2740834

[14] Wu, H., Pang, G. K. H., Choy, K. L., & Lam, H. Y. (2017). An optimization model for electric vehicle battery charging at a battery swapping station. *IEEE Transactions on Vehicular Technology*, *67*(2), 881-895. https://doi.org/10.1109/TVT.2017.2758404

[15] Tran, V. T., Islam, M. R., Muttaqi, K. M., & Sutanto, D. (2019). An efficient energy management approach for a solar-powered EV battery charging facility to support distribution grids. *IEEE Transactions on Industry Applications*, *55*(6), 6517-6526. https://doi.org/10.1109/TIA.2019.2940923

[16] Bist, V. & Singh, B. (2014). PFC Cuk converter-fed BLDC motor drive. *IEEE Transactions on Power Electronics*, *30*(2), 871-887. https://doi.org/10.1109/TPEL.2014.2309706

[17] Singh, B. & Kushwaha, R. (2019). A PFC Based EV Battery Charger Using a Bridgeless Isolated SEPIC Converter. *IEEE Transactions on Industry applications*, *56*(1), 477-487. https://doi.org/10.1109/TIA.2019.2951510

[18] Bist, V. & Singh, B. (2013). A reduced sensor PFC BL-Zeta converter based VSI fed BLDC motor drive. *Electric Power Systems Research*, *98*, 11-18. https://doi.org/10.1016/j.epsr.2013.01.006

Contact information:

Sajitha BALARAMAN
(Corresponding author)
SNS College of Engineering, SNS Kalvi Nagar,
Sathy Main Road, Kurumbapalayam, PO, Coimbatore, Tamil Nadu 641107, India
E-mail: sajitha.mpb@gmail.com

Vivekanandan CHENNIAPPAN
SNS College of Technology, SNS Kalvi Nagar,
Vazhiyampalayam, Saravanampatti Post, Coimbatore 641035, India
E-mail: vivekcit86@gmail.com